

Anomalous frequency and intensity scaling of collective and local modes in a coupled-spin tetrahedral system $\text{Cu}_2\text{Te}_2\text{O}_5\text{Cl}_2$

Kwang-Yong Choi

Department of Physics, Chung-Ang University, 221 Huksuk-Dong, Dongjak-Gu, Seoul 156-756, Republic of Korea

Hiroyuki Nojiri

Institute for Materials Research, Tohoku University, Katahira 2-1-1, Sendai 980-8577, Japan

Naresh S. Dalal

Department of Chemistry and Biochemistry, National High Magnetic Field Laboratory, Florida State University, Tallahassee, Florida 32306-4390, USA

Helmuth Berger

Institute de Physique de la Matiere Complexe, EPFL, CH-1015 Lausanne, Switzerland

Wolfram Brenig

Institute for Theoretical Physics, TU Braunschweig, D-38106 Braunschweig, Germany

Peter Lemmens

Institute for Condensed Matter Physics, TU Braunschweig, D-38106 Braunschweig, Germany

(Received 21 May 2008; revised manuscript received 18 August 2008; published 14 January 2009)

We report on the magnetic excitation spectrum of the coupled-spin tetrahedral system $\text{Cu}_2\text{Te}_2\text{O}_5\text{Cl}_2$ using Raman scattering on single crystals. The transition to an ordered state at $T_N^{\text{Cl}}=18.2$ K evidenced from thermodynamic data leads to the evolution of distinct low-energy magnetic excitations superimposed by a broad maximum. These modes are ascribed to magnons with different degree of localization and a two-magnon continuum. Two of the modes develop a substantial energy shift with decreasing temperature similar to the order parameter of other Néel ordered systems. The other two modes show only a negligible temperature dependence and dissolve above the ordering temperature in a continuum of excitations at finite energies. These observations point to a delicate interplay of magnetic intertetrahedra and intratetrahedra degrees of freedoms as expected for a system in the proximity to quantum criticality.

DOI: [10.1103/PhysRevB.79.024416](https://doi.org/10.1103/PhysRevB.79.024416)

PACS number(s): 78.30.-j, 75.40.Cx, 75.40.Gb

I. INTRODUCTION

Frustration and competition of magnetic interactions are one of the central concepts in condensed-matter physics.¹ It is related to unusual ground states and (quantum) criticality as well as exotic low-lying excitations. The latter may reach a fascinating complexity due to the dichotomy of local singlet versus collective magnon states. A prominent example is found in the three-dimensional (3D) pyrochlore lattice antiferromagnets (AF) consisting of corner-sharing tetrahedra. Such systems have a macroscopic number of classical ground states. Weak residual interactions of lattice and orbital origins lift these degeneracies in the limit to low temperatures.² Furthermore, order-by-disorder effects may be observed.

A weakly coupled counterpart of the pyrochlore system with $S=1/2$ is realized in the oxohalide $\text{Cu}_2\text{Te}_2\text{O}_5\text{X}_2$ ($X=\text{Br}, \text{Cl}$) and $\text{Cu}_4\text{Te}_5\text{O}_{12}\text{Cl}_{14}$ compounds.^{3,4} Four Cu^{2+} clusters form a distorted tetrahedron, which aligns in chains along the c axis. The tetrahedra are separated by lone-pair ions within the ab plane that allow an easy modification of the important in-plane exchange paths⁵ along oxygen and halogenoid ions using substitutions, chemical modifications,⁴ and pressure.^{6,7} Unlike the pyrochlore system, each tetrahe-

dron is isolated while still being coupled by intertetrahedral couplings. From spin topology point of view the arrangement of Cu^{2+} realizes all prerequisites for quantum criticality.

$\text{Cu}_2\text{Te}_2\text{O}_5\text{X}_2$ shows an incommensurate magnetic ordering at $T_N^{\text{Br}}=11.4$ K in $X=\text{Br}$ and $T_N^{\text{Cl}}=18.2$ K in $X=\text{Cl}$.^{8,9} The observed ordered magnetic moment $0.395(5)\mu_B$ of Cu^{2+} is strongly reduced for $X=\text{Br}$, compared to the classical value of $\sim 1\mu_B$.¹⁰ In contrast, for $X=\text{Cl}$ the moment of $0.88(1)\mu_B$ is closer to the saturated one. Since the unit-cell volume decreases by 7% as Br is substituted by Cl, the ratio between intratetrahedra and intertetrahedra couplings seems to be a crucial factor for understanding the respective magnetic behavior. Indeed, the *ab initio* calculation⁵ shows that exchange paths vary with composition because the Cl $3p$ orbital at the Fermi level is more strongly distorted toward the Cu $3d$ orbital than the Br $4p$ orbital. Moreover, for $X=\text{Cl}$ in-plane intertetrahedral diagonal interaction is estimated to be nearly as strong as the intratetrahedral interaction. With applied pressure $T_N^{\text{Br}}=11.4$ K is systematically reduced implying a decrease in the magnetic intertetrahedra coupling strengths and an enhanced degree of frustration.⁶ The effect of symmetry can be studied by comparing $\text{Cu}_2\text{Te}_2\text{O}_5\text{Cl}_2$ with $\text{Cu}_4\text{Te}_5\text{O}_{12}\text{Cl}_{14}$ as in the latter system the spin tetrahedra have a larger separation within the ab plane including an

inversion center.^{3,4} As a result it shows a more mean-field-like character of the magnetic properties.

In spite of the similar magnetic ordering structure of $\text{Cu}_2\text{Te}_2\text{O}_5\text{X}_2$ with $X=\text{Br}, \text{Cl}$, the detailed magnetic properties differ from each other. First, the effect of an external field and pressure on T_N is opposite.^{8,11} For $X=\text{Br}$, T_N decreases with increasing external field or pressure while for $X=\text{Cl}$ T_N increases with increasing field or pressure. Second, thermal conductivity differs from each other. The bromide shows a round maximum at low temperature, while the chloride displays a leveling-off followed by a steep increase for temperature below 15 K.^{12,13} Third, inelastic neutron-scattering (INS) measurements uncovered that the two compounds show a marked difference in the temperature dependence of magnetic excitations.¹⁴ For $X=\text{Br}$, upon heating the intensity of magnetic excitations decreases monotonically while undergoing no change in line shape. For $X=\text{Cl}$, however, the magnetic continuum shifts to lower energy and then evolves to a quasielastic diffusive response above T_N^{Cl} . This suggests that the nature of spin dynamics of both compounds is different.

In previous Raman investigations of $\text{Cu}_2\text{Te}_2\text{O}_5\text{Br}_2$ (Refs. 8, 15, and 16) various magnetic excitations have been observed in the spin singlet channel that provided evidence for the presence of a longitudinal magnon in this system. The latter is an important prerequisite for a proximity to quantum criticality.^{17,18} In contrast, the magnetic excitations of the $X=\text{Cl}$ system have not been fully addressed due to the lack of sizable single crystals. To enhance our understanding of this weakly interacting tetrahedral system and to differentiate the spin dynamics of $X=\text{Br}$ and Cl a thorough Raman spectroscopy investigation of $X=\text{Cl}$ is indispensable.

In this paper, we report dc magnetic susceptibility, high-field magnetization, and Raman-scattering measurements of large single crystals of $\text{Cu}_2\text{Te}_2\text{O}_5\text{Cl}_2$. The anisotropic magnetization suggests that the ground state is given by a long-range ordered state. However, we observe an intriguing richness of the magnetic Raman spectrum that consists of four sharp peaks as well as of a weaker broad continuum. The former are interpreted in terms of magnon excitation. The latter is due to two-magnon scattering whose temperature dependence is indicative of a minor contribution from localized fluctuations. The scaling of the modes points to a proximity of the compound to a quantum critical regime.

II. EXPERIMENTAL SETUP

Single crystals of $\text{Cu}_2\text{Te}_2\text{O}_5\text{Cl}_2$ were prepared by the halogen vapor transport technique, using TeCl_4 and Cl_2 as transport agents. Magnetic susceptibility was measured by a superconducting quantum interference device (SQUID) magnetometer (magnetic property measurement system (MPMS), Quantum Design). High-field magnetization measurements were carried out by means of a standard inductive method. A fast sweeping pulsed field was generated by a capacitor bank of 90 kJ.¹⁹ The sample is directly immersed in liquid ^3He to maintain a temperature of 0.4 K. Raman-scattering experiments were performed using the excitation line $\lambda = 514.5$ nm of an Ar^+ laser in a quasibackscattering

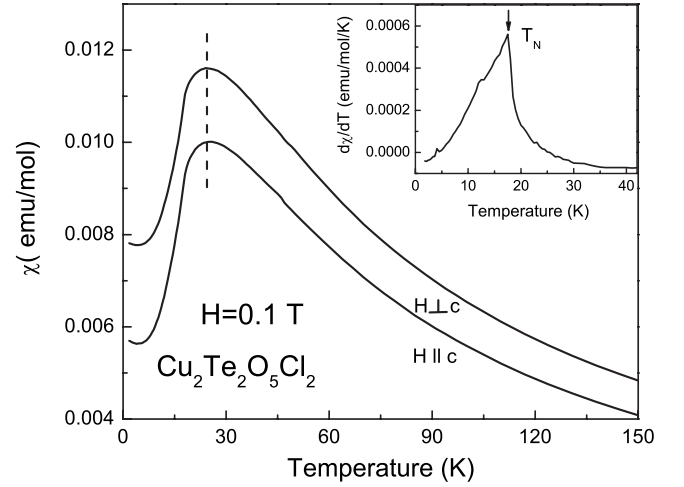


FIG. 1. Temperature dependence of magnetic susceptibility of $\text{Cu}_2\text{Te}_2\text{O}_5\text{Cl}_2$, $\chi(T)$, in an applied field of $H=0.1$ T for $H\parallel c$ and $H\perp c$ axes, respectively. Inset: derivative of magnetic susceptibility, $d\chi/dT$. The kink at $T_N^{\text{Cl}}=18.2$ K corresponds to long-range magnetic ordering.

geometry.²⁰ A comparably small laser power of 0.1 mW was focused to a 0.1 mm diameter spot on the surface of the single crystal in contact gas. The scattered spectra were collected by a DILOR-XY triple spectrometer and a nitrogen cooled charge-coupled device detector.

III. EXPERIMENTAL RESULTS

A. Magnetic susceptibility and magnetization

Figure 1 displays the temperature dependence of the magnetic susceptibility $\chi(T)$ in a field $H=0.1$ T for $H\parallel c$ and $H\perp c$ axes, respectively. Our results confirm earlier data.^{3,8,17,18,21} With decreasing temperature $\chi(T)$ shows a broad maximum around $T_{\text{max}}=24$ K. This is associated with the onset of short-range magnetic ordering. Upon further cooling, $\chi(T)$ exhibits a kink around 18.2 K and then drops to a finite residual value as $T\rightarrow 0$. The kink is identified with a transition to a long-range ordered state at $T_N^{\text{Cl}}=18.2$ K as evidenced by the λ -like anomaly of $d\chi/dT$ (see the inset of Fig. 1).

In Ref. 3 $\chi(T)$ was approximated in terms of an isolated tetrahedral model with a spin-gapped state of $\Delta \approx J_1 = J_2 \sim 38.5$ K, where J_1 and J_2 are the two intratetrahedral exchange interactions. However, it is difficult to extract accurately the exchange interactions and spin gap from an analysis of $\chi(T)$ since significant intertetrahedral couplings smear out the spin gap features.^{5,18,22,23} Actually, $\chi(T)$ becomes slightly anisotropic for temperatures below T_{max} due to the onset of long-range correlations. In addition, $\chi(T)$ approaches a finite value as $T\rightarrow 0$ without falling to zero. This suggests that the spin gap is filled with dense singlet-triplet mixed states leading to a finite magnetization.

Shown in Fig. 2 is the high-field magnetization. We observe an anisotropic magnetization behavior. For fields applied perpendicular to the c axis, the magnetization displays a linear field dependence, i.e., the susceptibility is field inde-

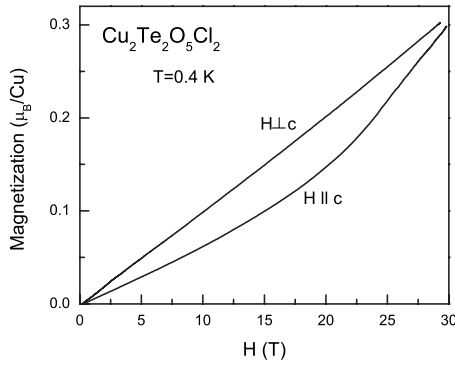


FIG. 2. High-field magnetization of $\text{Cu}_2\text{Te}_2\text{O}_5\text{Cl}_2$ for $H \parallel c$ and $H \perp c$ axes at $T=0.4$ K, respectively, measured using a pulsed magnetic field.

pendent. In contrast, for field applied along the c axis the magnetization is reduced with a concave curvature in the studied field interval up to 30 T. We recall that a magnetization plateau at half the saturation value has been predicted for a linear chain of spin tetrahedra in a spin-gapped ground state.²⁴ The absence of a half-magnetization plateau together with the anisotropy suggests that the ground state is governed by a classically ordered state rather than by a spin singlet state. On a qualitative level, the anisotropic magnetization behavior is compatible with helical magnetic ordering. The linear field dependence for $H \perp c$ is associated with an easy-plane-type magnetization. The change in the magnetization slope for $H \parallel c$ might be related to a spin-flop transition with an incommensurate wave vector.

B. Raman scattering

The low-energy Raman spectra of $\text{Cu}_2\text{Te}_2\text{O}_5\text{Cl}_2$ are displayed in Fig. 3 for (cc) , (aa) , (ca) , and (ab) polarizations at 3 K. $\text{Cu}_2\text{Te}_2\text{O}_5\text{Cl}_2$ has the space group $F\bar{4}$ with two formula units per unit cell. Subtracting the acoustic modes the factor group analysis yields a total of 49 Raman-active modes; $\Gamma_{\text{Raman}} = 16A(aa+bb, cc) + 16B(aa-bb, ab) + 17E(ac, bc)$. At room temperature we observe 44 peaks in the frequency regime 80–700 cm^{-1} as phonon scattering. The missing of few modes is attributed to their weak intensity or degeneracy in energy with other excitations. No distinct phonon anomalies as frequency shifts or changes of the phonon linewidth are found in a wide temperature range. Similar observations have been made for the other tetrahedra based compounds.^{4,8,16,17} Thus, we omit a further discussion of the phonon modes.

Hereafter, we will focus on the magnetic excitations which differ from the phonons by their characteristic energy scale and the variations in both intensity and energy with temperature. These excitations are composed of four peaks at 23 ($M1$), 39 ($M2$), 49 ($M3$), and 67 cm^{-1} ($M4$) superimposed on a weak broad continuum ($2M$) extending from 30 to 120 cm^{-1} (see Fig. 5). The magnetic modes are observed for all polarizations with only a very moderate symmetry dependence suggesting that they contribute to all possible A , B , and E symmetries. This is related to the three-dimensional

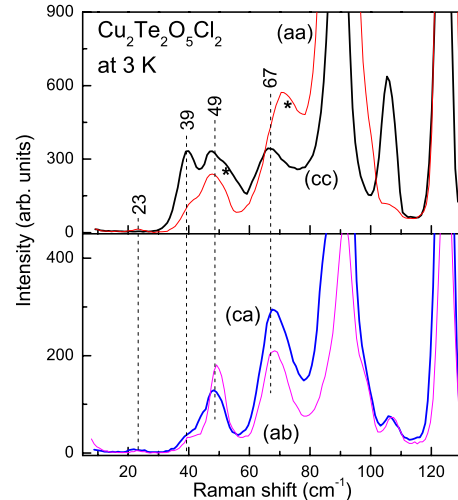


FIG. 3. (Color online) Low-frequency Raman spectra of $\text{Cu}_2\text{Te}_2\text{O}_5\text{Cl}_2$ for (cc) , (aa) , (ca) , and (ab) polarizations at $T=3$ K. The dashed lines denote the position of four magnetic signals. The numbers give their respective energies in the unit cm^{-1} . The asterisks denote low-frequency phonon modes that superimpose the magnetic signals.

network of spin tetrahedra and antisymmetric Dzyaloshinsky-Moriya interactions which may release Raman-scattering selection rules.^{18,25}

In Fig. 4 the detailed temperature dependence of Raman-scattering data in (ab) polarization of $\text{Cu}_2\text{Te}_2\text{O}_5\text{Cl}_2$ is displayed. Above the magnetic ordering temperature the low-energy magnetic excitations dissolve into a continuum of excitations at finite energies. Upon further heating, an additional quasielastic signal (QC) is observed. For a quantitative analysis we fit them (Mi and $2M$) to Gaussian profiles by taking into account four phonon peaks (Pi). The representative fit is displayed in Fig. 5. One-magnon-like excitations are light scattering processes by magnons at the Brillouin zone center. Like other scattering processes, thus, a Gaussian

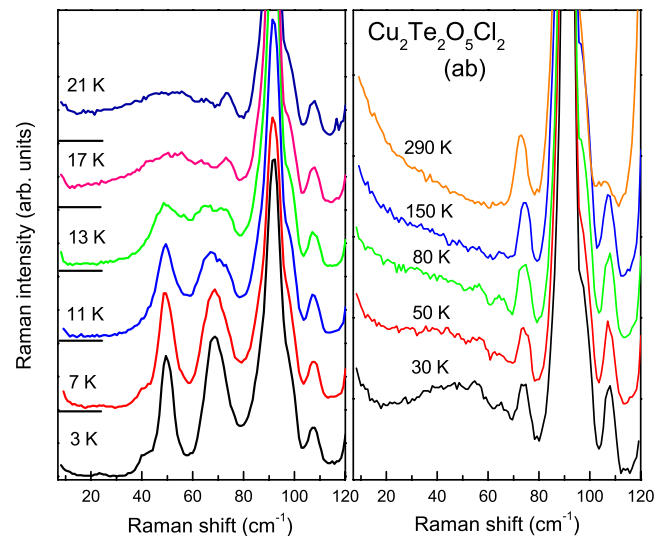


FIG. 4. (Color online) Temperature dependence of low-frequency Raman spectra in (ab) polarization.

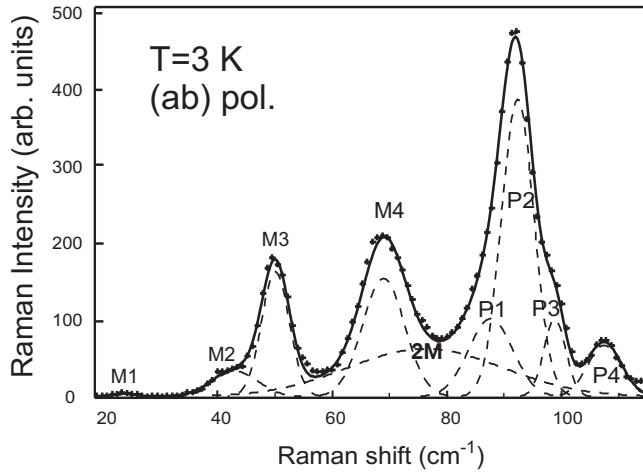


FIG. 5. Representative fit of $\text{Cu}_2\text{Te}_2\text{O}_5\text{Cl}_2$ at 3 K to Gaussian profiles. M_i ($i=1-4$), $2M$, and P_i ($i=1-4$) correspond to the four sharp magnetic signals, the two-magnon continuum, and the four optical phonons, respectively. The crosses denote the raw data, the solid line the total sum of a fitting, and the dashed lines an individual fitting.

profile provides the most reliable fitting. However, no analytic form is known for a two-magnon continuum. Nonetheless, in the studied compound a Gaussian profile can serve as a good approximation. We note that the sister compound $\text{Cu}_2\text{Te}_2\text{O}_5\text{Br}_2$ shows a gapped symmetric two-magnon-like continuum.⁸ Due to enhanced intertetrahedral exchange interactions this feature is expected to be rounded off in $\text{Cu}_2\text{Te}_2\text{O}_5\text{Cl}_2$. Our assumption is corroborated by the energy scale and spectral range of the obtained continuum. Compared to the bromide, the continuum in the chloride broadens and its peak position shifts to higher energy. This is fully consistent with the increased intertetrahedral exchange interactions. The resulting peak frequencies and intensities are depicted in Fig. 6 on a logarithmic temperature scale and in Fig. 7 on a log-log plot as a function of the reduced temperature, $t=1-T/T_N$. The errors are of the symbol size.

The intensity as well as the energy of modes $M1$ - $M4$ is renormalized to a different extent with increasing temperatures. This evolution can be used to characterize the modes in addition to their absolute frequencies. While the intensities of $M1$ and $M2$ are comparably small and drop too fast to allow a detailed analysis, the modes $M3$ and $M4$ show a moderate decrease in intensity following a more rapid drop in the proximity of T_N . In contrast, the two-magnon scattering intensity increases and even forms a maximum at 25 K, i.e., very close to the maximum in the magnetic susceptibility. This increase in the scattering continuum resembles observations in the strongly frustrated, two-dimensional (2D) Shastry-Sutherland system $\text{SrCu}_2(\text{BO}_3)_2$. In the latter system it is due to the localization of triplet excitations on a strongly frustrated lattice with a temperature-independent spin gap.²⁶ It is noteworthy that in the latter system the intensity drops to zero for small temperatures while in the spin tetrahedron case finite intensity remains.

Dividing the intensity of magnetic quasielastic scattering ($\Delta\omega \approx 0$) by T^2 leads to a measure of the fluctuations of the magnetic energy density. This quantity is proportional to the

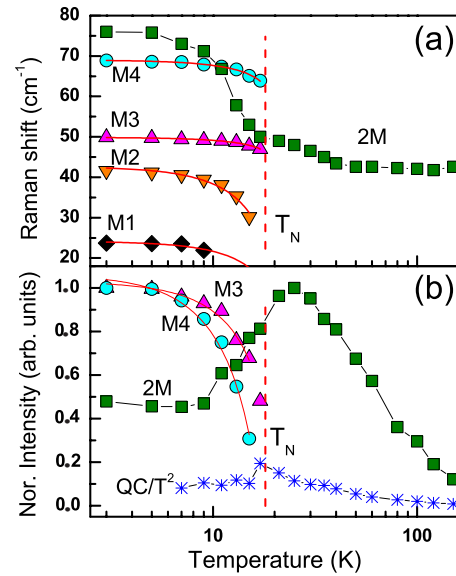


FIG. 6. (Color online) (a) Peak frequency of the magnetic signals, M_i ($i=1-4$) and the two-magnon continuum; $2M$ for $\text{Cu}_2\text{Te}_2\text{O}_5\text{Cl}_2$ on a logarithmic temperature scale. (b) Scattering intensity of the magnetic signals. The intensity of quasielastic scattering, QC, is normalized by T^2 to be compared with the magnetic specific heat (Ref. 8). Lines are guides for the eyes.

specific heat of a quantum spin system²⁷ as also observed in $\text{SrCu}_2(\text{BO}_3)_2$.²⁶ The proportionality considers the Bose factor in $\text{Im}[\chi(\omega)]$ in the low-frequency and high-temperature limits. In the lower panel of Fig. 6 this renormalized intensity is plotted for $\text{Cu}_2\text{Te}_2\text{O}_5\text{Cl}_2$ with a sharp maximum at T_N which is similar to the earlier reported specific-heat data.⁸

With respect to energy the peak frequencies of the modes $M3$ and $M4$ behave different from $M1$ and $M2$. The renormalization for $T < T_N$ is less pronounced and more steplike at

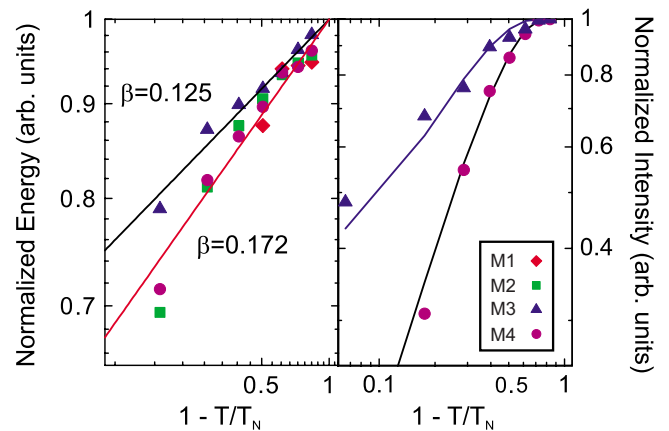


FIG. 7. (Color online) Log-log plots of the normalized energy and frequency of magnetic scattering in $\text{Cu}_2\text{Te}_2\text{O}_5\text{Cl}_2$ as a function of the reduced temperature, $t=1-T/T_N$. The results of the individual fits are given in Table I. (Left panel) Normalized energy $(E-E_0)/E_{\text{max}}$ as a function of temperature for the modes $M1$ - $M4$. (Right panel) Normalized intensity, I/I_{max} , as a function of t for the modes $M3$ and $M4$ compared to a Boltzmann related scattering factor (full lines) taking the temperature dependence of the populated energy levels into account.

TABLE I. Results of fitting the energy of the four magnetic peaks to a scaling function of $(E-E_0)/E_{\max}=t^\beta$.

Mode	E_0+E_{\max} (cm^{-1})	E_0 (cm^{-1})	E_{\max} (cm^{-1})	β
<i>M1</i>	25	0	25	0.147
<i>M2</i>	43.5	0	43.5	0.193
<i>M3</i>	50.1	39.1	11	0.125
<i>M4</i>	69.5	54.1	15.4	0.172

$T=T_N$ resembling the effect of a first-order-like phase transition on the order parameter. In contrast to *M1-M4* the *2M* energy does not soften completely from its low-temperature maximum of approximately 76 cm^{-1} . For temperatures above T_N^{Cl} there is still a finite-energy spectral weight at 41 cm^{-1} [see Fig. 6(a)].

Comparing these observations with the generic behavior of local magnetic exchange scattering of an AF system²⁸ leads to the following conclusions: with respect to energy the sudden drop in energy and disappearance of the modes *M3* and *M4* are anomalous as well as the nearly constant energy of *2M* for temperatures $T>T_N$. With respect to intensity especially the behavior of *2M* is noteworthy. In conventional AF the intensity of exchange scattering survives several times the Néel temperature without showing an anomalous enhancement. All our experimental results are consistent with the persistence of finite-energy short-range correlations, i.e., a gapped energy spectrum in the temperature regime $T>T_N$.

In Fig. 7 we show a scaling analysis of the peak energies and intensities by log-log plots as a function of $t=1-T/T_N$.²⁹ The full lines in the left panel correspond to a critical behavior with the exponents $\beta=0.125$ and 0.172 in $(E-E_0)/E_{\max}=t^\beta$, with the temperature-independent energy offset or gap E_0 . It is clear from the previous discussion that *M3* and *M4* can only be described taking a finite offset E_0 into account. The same would be valid for the *2M* energy; however, we have omitted this signal from the analysis because of its broader linewidth. To evaluate a scaling of *M1* and *M2* this offset is not needed. Therefore the latter two modes show a seemingly larger renormalization in the available temperature range. The detailed results of the individual fits for $T=0$ are given in Table I.

In the right panel of Fig. 7 we have analyzed the intensity of *M3* and *M4* omitting the other two signals due to their smaller intensities and sharp drop with rising temperatures. It is obvious that a description of the intensity using a power law is not satisfying. Therefore we used a model that has been successfully applied to the intensity of bound states in $\text{SrCu}_2(\text{BO}_3)_2$.²⁶ In this approach the modes are suppressed due to thermal fluctuations taking the occupation of the modes and their temperature dependence into account. This leads to a fit with essentially one free parameter, a scattering efficiency A , as a prefactor of the Boltzmann term. The normalized intensity of *M3* and *M4* is therefore proportional to $I_B(T) \propto 1 - A e^{-\Delta(T)/k_B T}$, with $\Delta(T)$ given by the temperature-dependent peak energy *M3* or *M4*, with $A=9$ and 0.5 , respectively. This indicates that the rigidity of the modes *M3*

and *M4* is determined by thermal fluctuations as the bound states of $\text{SrCu}_2(\text{BO}_3)_2$ do. Such a behavior is not characteristic of the magnetic modes related to an order parameter.

We relate the temperature-dependence peak energies to the evolution of intertetrahedral correlations with the onset of ordering at $T \leq T_N^{\text{Cl}}$. The transversal triplet excitation observed in neutron scattering on the spin chain system CuGeO_3 below its spin-Peierls transition shows a similar behavior.³⁰

The reduced critical exponents $\beta=0.125-0.172$ of *M3* and *M4* are considerably smaller than a mean-field value of $\beta=0.5$ expected for a conventional magnetic phase transition. This together with finite E_0 suggests that both *M3* and *M4* modes should not be ascribed to the order parameter but to spin singlet fluctuations arising from isolated spin tetrahedra. The corresponding energy scale is not so well established and band-structure calculations point to a similar order of magnitude of the intertetrahedral interactions.⁵ A rough approximation could be given by a fit to the magnetic susceptibility with an isolated tetrahedral model leading to $J=38.4 \text{ K}$.^{3,4} For $X=\text{Br}$ there exists also a high-energy mode with very weak temperature dependence. This triangular broadened mode might be understood as composed of several modes, i.e., an overlap of *M3* and *M4* of $\text{Cu}_2\text{Te}_2\text{O}_5\text{Cl}_2$. Although the higher-energy modes in the two systems show several similarities, there is one major difference in the behavior at higher temperatures, $T>T_N$. While the broad triangular mode for $X=\text{Br}$ survives several times T_N , the sharp modes for $X=\text{Cl}$ rapidly disappear and dissolve in the broader *2M* signal. The interpretation of this difference is not straightforward and could be due to a weakly first-order contribution to the phase transition in $\text{Cu}_2\text{Te}_2\text{O}_5\text{Cl}_2$.

Anticipating the latter detailed discussion, we summarize that our study unveils a survival of zero-dimensional quantum fluctuations attributed to individual spin tetrahedra even though at lower temperatures long-range ordering takes place due to the coupling of the spin entities.

C. Comparison of neutron and Raman scattering

In the following we will compare Raman scattering (Fig. 4 of Ref. 8) with neutron scattering [Fig. 7(a) of Ref. 14] addressing first the results for $X=\text{Br}$. Two components of the magnetic excitation spectrum have been observed in neutron scattering: (i) a flat constant energy component and (ii) a dispersive excitation. In a coupled tetrahedra system localized, dispersionless excitations are expected to occur due to intratetrahedral interactions and dispersive excitations due to intertetrahedral coupling. In this light, the former is related to a spin gap feature while the latter to an incommensurate magnetic ordering. The simultaneous observation of two components points to the coexistence of long-range order with a spin-gapped ground state. As discussed before, in Raman scattering a strongly temperature dependent and a weakly temperature-dependent feature exist. The small shift of the latter signal is due to the damping of a Goldstone mode. Since the softened spectral weight is small, we conclude that the ground state and spin dynamics of $X=\text{Br}$ is governed by spin singlet fluctuations. This is supported by

the strongly reduced magnetic moment $0.395(5)\mu_B$ of Cu^{2+} .¹⁰ For temperatures above T_N^{Br} the intensity of the continuum is monotonically suppressed without any change in line shape.

The similarity of the spectral response in INS and Raman scattering is a striking feature considering different mechanisms for the scattering processes. Raman spectroscopy probes simultaneous two-spin-flip processes leading to a two-magnon continuum. Thus, the magnetic continuum is proportional to twice the magnon density of states. In contrast, INS corresponds to a spin-spin correlation function in momentum space. As the available INS experiments have been performed on polycrystalline samples the close correspondence between the two spectroscopic results might be based on the averaging of the INS intensity over momentum space. This intensity is roughly given by the one-magnon density of state.

Next, we turn to the discussion of the chloride. INS shows a magnetic excitation spectrum that again consists of two components, that is, a flat dispersionless band at 6 meV (48 cm^{-1}) and a dispersive lower-energy component. Its energy scale is smaller, 3 meV (24 cm^{-1}), and has a gap of 2 meV (16 cm^{-1}).³¹ INS on a polycrystalline sample shows a progressive shift of spectral weight to lower energy with increasing temperature and its transfer to a QC diffusive response in the paramagnetic state [compare Figs. 4 and 7(b) of Ref. 14]. More recently it has been shown that the dispersive mode partially softens and remains gapped while being further broadened.³¹ The softening of the magnetic excitation implies the damping of short-range magnetic fluctuations by thermal fluctuations.³² Therefore, we conclude that the spin dynamics of $X=\text{Cl}$ is dominated by long-range ordering in contrast to the case with $X=\text{Br}$. This is consistent with the larger ordered moment of $0.88(1)\mu_B$ in $X=\text{Cl}$.

D. Analysis of the magnetic Raman scattering

Here we will discuss several options for the potential origin of the four sharp peaks at 23 ($M1$), 39 ($M2$), 49 ($M3$), and 67 cm^{-1} ($M4$). As shown in Fig. 6, the peaks shift to lower frequency with increasing temperature and vanish on the low-temperature side of T_N . Thus, they might originate from a transverse magnon excitation at $q=0$.

Another possible interpretation is in terms of a longitudinal magnon. Such excitations have been observed in Raman-scattering experiments of the sister compound of $X=\text{Br}$. To be more specific we start by considering the eigenstates of the isolated tetrahedron at site \mathbf{r} with Hamiltonian $H(\mathbf{r}) = J_1[(\mathbf{S}_{\mathbf{r}1} + \mathbf{S}_{\mathbf{r}2}) \cdot (\mathbf{S}_{\mathbf{r}3} + \mathbf{S}_{\mathbf{r}4})] + J_2(\mathbf{S}_{\mathbf{r}1} \cdot \mathbf{S}_{\mathbf{r}2} + \mathbf{S}_{\mathbf{r}3} \cdot \mathbf{S}_{\mathbf{r}4})$. These consist of two singlets $s_{1,2}$, at least one of which is the ground state, three triplets $t_{1,2,3}^\alpha$, and one quintuplet q^α . At $J_1 = J_2$ the two singlets form a degenerate ground state. While $J_1 \approx J_2$ applies to $X=\text{Cl}$, we assume $J_2 < J_1$ for definiteness and s_1 to be the ground state. This is similar to $X=\text{Br}$. The actual

structure of the intertetrahedral coupling in the tellurates is an open issue, but to a first approximation it may be modeled by a molecular field $H_{\text{MF}} = \sum_{\mathbf{r}l} \mathbf{M}_{\mathbf{r}l} \cdot \mathbf{S}_{\mathbf{r}l}$ with some incommensurate order parameter $\mathbf{M}_{\mathbf{r}l}$ for $T < T_N$.^{9,10} As suggested by the analysis in Refs. 17 and 18, H_{MF} will mix the ground-state singlet with the triplet components along the local quantization axis of the molecular field. *A priori*, such mixing does not have to be restricted to only one of the triplets, as in Ref. 17, but may involve all three. Discarding the high-energy quintuplet this would imply four low-energy excited states directly observable at zero-momentum transfer by Raman scattering, i.e., one singlet s_2 at energy $2J_1 - 2J_2$ and three longitudinal magnons which vanish above T_N . The 3×2 transverse triplets contribute to the two-magnon scattering continuum only. This sets in at higher energies and remains unaffected by the transition at T_N , as for the remaining one-magnon and two-magnon contributions from the quintuplet.

From this one should conclude first, that one of the four modes $M1$ - $M4$ corresponds to the excited singlet. In comparison to the 23.2 cm^{-1} mode for $X=\text{Br}$, $M1$ would be a likely candidate for this, leaving $M2$ - $M4$ for the longitudinal magnons. Second, the singlet mode among $M1$ - $M4$ should be affected only weakly by an external magnetic field, while the remaining three should be field dependent through their triplet admixture. This should be investigated by future Raman studies in finite magnetic fields. Finally, for a second-order transition the longitudinal magnon energies should vanish as $T \rightarrow T_N$ for $T < T_N$. However, while some softening is observable in all of the modes in Fig. 6, their behavior would be more indicative of a weakly first-order transition. Indeed and depending on the molecular field, first-order transitions may occur for coupled tetrahedral, as already noted in the comment under Ref. 12 of Ref. 17.

IV. CONCLUSIONS

To conclude, we have presented magnetic susceptibility, high-field magnetization, and Raman-scattering studies of the coupled-spin tetrahedral system $\text{Cu}_2\text{Te}_2\text{O}_5\text{Cl}_2$. Several distinct magnetic excitations are observed as one-magnon modes in addition to a two-magnon continuum. The exceptionally rich magnetic excitation spectrum evidences the significance of a localized spin singlet dynamics arising from zero-dimensional spin tetrahedra topology even though the static ordered moment has nearly a classical value.

ACKNOWLEDGMENTS

This work was supported by the German Science Foundation and the ESF program Highly Frustrated Magnetism. Work at the EPFL was supported by the Swiss NSF and by the NCCR MaNEP. Work at FSU was supported by NSF (Grant No. DMR-0506946). We acknowledge important discussions with R. Valentí.

- ¹See, for example, *Magnetic Systems with Competing Interactions*, edited by H. T. Diep (World Scientific, Singapore, 1994); John E. Greedan, *J. Mater. Chem.* **11**, 37 (2001); R. Moessner and A. P. Ramirez, *Phys. Today* **59**, 24 (2006); C. Lhuillier, arXiv:cond-mat/0502464 (unpublished).
- ²O. Tchernyshyov, R. Moessner, and S. L. Sondhi, *Phys. Rev. B* **66**, 064403 (2002).
- ³M. Johansson, K. W. Tornroos, F. Mila, and P. Millet, *Chem. Mater.* **12**, 2853 (2000).
- ⁴R. Takagi, M. Johansson, V. Gnezdilov, R. K. Kremer, W. Brenig, and P. Lemmens, *Phys. Rev. B* **74**, 014413 (2006).
- ⁵R. Valentí, T. Saha-Dasgupta, C. Gros, and H. Rosner, *Phys. Rev. B* **67**, 245110 (2003).
- ⁶J. Kreitlow, S. Süllow, D. Menzel, J. Schoenes, P. Lemmens, and M. Johansson, *J. Magn. Magn. Mater.* **290-291**, 959 (2005).
- ⁷X. Wang, I. Loa, K. Syassen, P. Lemmens, M. Hanfland, and M. Johansson, *J. Phys.: Condens. Matter* **17**, S807 (2005); X. Wang, I. Loa, K. Syassen, and P. Lemmens (unpublished).
- ⁸P. Lemmens, K.-Y. Choi, E. E. Kaul, C. Geibel, K. Becker, W. Brenig, R. Valentí, C. Gros, M. Johansson, P. Millet, and F. Mila, *Phys. Rev. Lett.* **87**, 227201 (2001).
- ⁹O. Zaharko, A. Daoud-Aladine, S. Streule, J. Mesot, P.-J. Brown, and H. Berger, *Phys. Rev. Lett.* **93**, 217206 (2004).
- ¹⁰O. Zaharko, H. Rønnow, J. Mesot, S. J. Crowe, P. J. Brown, A. Daoud-Aladine, A. Meents, A. Wagner, M. Prester, H. Berger, and D. M. Paul, *Phys. Rev. B* **73**, 064422 (2006).
- ¹¹S. J. Crowe, M. R. Lees, D. M. Paul, R. I. Bewley, J. Taylor, G. McIntyre, O. Zaharko, and H. Berger, *Phys. Rev. B* **73**, 144410 (2006).
- ¹²M. Prester, A. Smontara, I. Zivkovic, A. Bilusic, D. Drobac, H. Berger, and F. Bussy, *Phys. Rev. B* **69**, 180401(R) (2004).
- ¹³A. V. Sologubenko, R. Dell'Amore, H. R. Ott, and P. Millet, *Eur. Phys. J. B* **42**, 549 (2004).
- ¹⁴S. J. Crowe, S. Majumdar, M. R. Lees, D. McK. Paul, R. I. Bewley, S. J. Levett, and C. Ritter, *Phys. Rev. B* **71**, 224430 (2005).
- ¹⁵P. Lemmens, K.-Y. Choi, A. Ionescu, J. Pommer, G. Güntherodt, R. Valentí, C. Gros, W. Brenig, M. Johansson, P. Millet, and F. Mila, *J. Phys. Chem. Solids* **63**, 1115 (2002).
- ¹⁶P. Lemmens, K.-Y. Choi, G. Güntherodt, M. Johansson, P. Millet, C. Gros, and W. Brenig, *Physica B* **329-333**, 1049 (2003).
- ¹⁷C. Gros, P. Lemmens, M. Vojta, R. Valentí, K.-Y. Choi, H. Kageyama, Z. Hiroi, N. V. Mushnikov, T. Goto, M. Johansson, and P. Millet, *Phys. Rev. B* **67**, 174405 (2003).
- ¹⁸J. Jensen, P. Lemmens, and C. Gros, *Europhys. Lett.* **64**, 689 (2003).
- ¹⁹H. Nojiri, K.-Y. Choi, and N. Kitamura, *J. Magn. Magn. Mater* **310**, 1468 (2007).
- ²⁰P. Lemmens and K. Y. Choi, in *Encyclopedia of Condensed Matter Physics*, edited by G. Bassani, G. Liedl, and P. Wyder (Elsevier, Amsterdam, 2005).
- ²¹Z. Jaglicic, S. El Shawish, A. Jeromen, A. Bilusic, A. Smontara, Z. Trontelj, J. Bonca, J. Dolinsek, and H. Berger, *Phys. Rev. B* **73**, 214408 (2006).
- ²²M.-H. Whangbo, J.-J. Koo, D. Dai, and D. Jung, *Inorg. Chem.* **42**, 3898 (2003).
- ²³W. Brenig, *Phys. Rev. B* **67**, 064402 (2003).
- ²⁴K. Totsuka and H.-J. Mikeska, *Phys. Rev. B* **66**, 054435 (2002).
- ²⁵V. N. Kotov, M. E. Zhitomirsky, M. Elhajal, and F. Mila, *Phys. Rev. B* **70**, 214401 (2004); V. N. Kotov, M. E. Zhitomirsky, M. Elhajal, and F. Mila, *J. Phys.: Condens. Matter* **16**, S905 (2004).
- ²⁶P. Lemmens, M. Grove, M. Fischer, G. Güntherodt, V. N. Kotov, H. Kageyama, K. Onizuka, and Y. Ueda, *Phys. Rev. Lett.* **85**, 2605 (2000).
- ²⁷P. Lemmens, G. Güntherodt, and C. Gros, *Phys. Rep.* **375**, 1 (2003).
- ²⁸M. G. Cottam and D. J. Lockwood, *Light Scattering in Magnetic Solids* (Wiley-Interscience, New York, 1986).
- ²⁹In Raman scattering on a large semitransparent crystal of CuGeO_3 and otherwise similar experimental conditions, we have estimated a local heating of the samples of 0.5 K/mW around $T=14$ K and an error of the temperature sensor of ± 0.5 K. We have tested the effect of a moderate change in T_N in the power-law fits leading to an approximate error of 10%–20% in β .
- ³⁰M. Nishi, O. Fujita, and J. Akimitsu, *Phys. Rev. B* **50**, 6508 (1994).
- ³¹S. Streule (private communication); S. Streule, H. M. Ronnow, Ch. Niedermayer, H. Berger, and J. Mesot, SINQ Progress Report No. II/04-S-97. 2005
- ³²K.-Y. Choi, S. A. Zvyagin, G. Cao, and P. Lemmens, *Phys. Rev. B* **69**, 104421 (2004) and references therein.